Proceedings of ASME Turbo Expo 2011
GT2011
June 6-10, 2011, Vancouver, British Columbia, Canada

GT2011-46784

ENGINE DESIGN STRATEGIES TO MAXIMIZE CERAMIC TURBINE LIFE AND RELIABILITY

Michael J. Vick
U.S. Naval Research Laboratory
Washington, D.C. 20375 USA

Osama M. Jadaan
University of Wisconsin-Platteville
Platteville, WI 53818 USA

Andrew A. Wereszczak
Oak Ridge National Laboratory
Oak Ridge, TN 37831-6062 USA

Sung R. Choi
Naval Air Systems Command
Patuxent River, MD 20670 USA

Andrew L. Heyes
Imperial College London
London SW7 2AZ UK

Keith R. Pullen
City University London
London EC1V 0HB UK

ABSTRACT

Ceramic turbines have long promised to enable higher fuel efficiencies by accommodating higher temperatures without cooling, yet no engines with ceramic rotors are in production today. Studies cite life, reliability, and cost obstacles, often concluding that further improvements in the materials are required. In this paper, we assume instead that the problems could be circumvented by adjusting the engine design. Detailed analyses are conducted for two key life-limiting processes, water vapor erosion and slow crack growth, seeking engine design strategies for mitigating their effects. We show that highly recuperated engines generate extremely low levels of water vapor erosion, enabling lives exceeding 10,000 hours, *without* environmental barrier coatings. Recuperated engines are highly efficient at low pressure ratios, making low blade speeds practical. Many ceramic demonstration engines have had design point mean blade speeds near 550 m/s. A CARES/Life analysis of an example rotor designed for about half this value indicates vast improvements in SCG-limited life and reliability. Lower blade speeds also reduce foreign object damage (FOD) particle kinetic energy by a factor of four. In applications requiring very high fuel efficiency that can accept a recuperator, or in short-life simple cycle engines, ceramic turbines are ready for application today.

INTRODUCTION

Over a billion dollars have been spent on ceramic turbine research and development, but ceramic turbines "have not yet reached bill-of-materials status" [1]. Mature turbine-grade silicon nitrides (e.g. SN282[1], AS800[2], SN88[3], NT154[4]) have excellent properties, but studies still cite life, reliability, and cost issues, often concluding that the materials themselves require further improvement. However, under less severe operating conditions, ceramics can excel in all these areas. In an ongoing long-term endurance test at NRL, a low cost porcelain vessel has been subjected to the thermal shock of hot coffee several times daily for ten years – over 5,000 startup/shutdown cycles – with no perceptible degradation. Ceramic turbocharger rotors have been manufactured for the notoriously cost-sensitive automotive market at rates exceeding 10,000 per month, achieving good life and reliability in Japanese sports cars. These examples suggest that rather than just seeking higher-performance materials, it might also be fruitful to design gas turbines to create a more benign environment for existing ceramics.

Foremost among stated concerns is water vapor erosion [2-11], a process in which water in the combustion products reacts with silicon nitride at high temperatures, forming gases that get swept away by the freestream. This erodes the blade surfaces at a rate "far beyond acceptable long term limits" [2]. However, conditions controlling the recession rate vary widely among engine designs, a fact that is usually neglected. For example, a common assumption in the water vapor studies is that "[t]he combustion environment for hydrocarbon/air systems contains ~10% water vapor, independent of hydrocarbon type and fuel-to-air ratio" [3]; [11, 12]. Actually, we show in this paper that the water vapor content of lean combustion products is strongly dependent on both the fuel and

[1] Kyocera Industrial Ceramic Components, Vancouver, WA

[2] Honeywell Ceramic Components, Torrance, CA
[3] NGK Insulators Ltd., Nagoya, Japan
[4] Saint-Gobain Ceramics and Plastics, Northboro, MA

the air/fuel ratio. For a typical recuperated microturbine operating at a Jet-A air/fuel equivalence ratio of 7.6, at 15°C and 50% relative humidity, the water vapor content is only 2.6%. The erosion rate is proportional to water vapor partial pressure *squared*, and thus is almost sixteen times lower than the 10% rule of thumb would suggest.

Similarly, most ceramic demonstration engines have had design point mean blade speeds in the 500-600 m/s range. The problems that control the life, reliability, and cost of ceramic turbines are all strongly influenced by the blade speed. For example, the critical flaw size to initiate fast fracture is proportional to the square of the applied stress, which in turn is proportional to the square of the blade speed. Thus, halving the blade speed should increase the critical flaw size by a factor of sixteen. The same strategy might therefore be expected to reduce slow crack growth (SCG) rates by a large factor as well.

Lower blade speeds also reduce the probability of foreign object damage (FOD), which can be a major problem at the high blade and gas speeds typical in gas turbine engines [13-16]. Since FOD particle kinetic energy ($\frac{1}{2}mV^2$) controls the probability of impact damage, halving the blade speed should quadruple the limiting particle mass that an engine could ingest without damage.

In this paper, we analyze water vapor erosion in detail, showing that lives in the tens of thousands of hours are achievable, without EBCs, in low pressure ratio recuperated engines. We show that this type of engine can employ very low blade speeds (220-350 m/s) without compromising simplicity, practicality, or efficiency. We then present a detailed analysis of slow crack growth. Using CARES/*Life* software, we demonstrate that low blade speeds lead to major improvements in life and reliability. Next, we briefly discuss the likely effects on FOD vulnerability and cost. Finally, we juxtapose the erosion-limited life estimates with efficiency and specific work calculations from a cycle model, in an attempt to identify markets where ceramic turbines could be viable today.

WATER VAPOR EROSION

Silicon nitride oxidizes at its surface, forming a silica layer that combines with water vapor at high temperatures to form gaseous products, according to the following reactions [5]:

$$Si_3N_4 + 6H_2O \rightarrow 3SiO_2 + 2N_2(g) + 6H_2(g) \quad (1)$$

$$SiO_2(s) + 2H_2O(g) \rightarrow Si(OH)_4(g) \quad (2)$$

The gases diffuse through the boundary layer and get swept away by the freestream, eroding the blade surface. Once the silica layer thickness reaches a steady state value, often after only a few hours, the surface recesses at a constant rate controlled by the boundary layer gas diffusion process.

Standard model

For a given specimen geometry and measurement method, the erosion rate has been predicted successfully [2, 3, 5-8] by:

$$\dot{y}_l = B_1 \frac{V^{0.5} P_{H2O}^2}{P_{total}^{0.5}} \exp\left(\frac{-Q}{RT}\right) \quad (3)$$

where:

$\dot{y}_l$ is the recession rate (μm/hr)
B_1 is a material constant (μm/hr) / ([m/s]$^{.5}$bar$^{1.5}$)
V is the local gas velocity (m/s)
P_{H2O} is the water vapor partial pressure (bar)
P_{total} is the total gas pressure (bar)
Q is an activation energy (-108,000 J/mol per [2, 6, 7])
R is the universal gas constant (8.314 J/mol-K)
T is the local gas temperature (K)

The constant B_1 must be calibrated from test results for a given material. Two exhaustive sets of experiments, summarized in Table 1, are suitable for this purpose. Tests 1 and 4, described in [7] and [8], were performed in a Rolls-Royce model 501-K[5] gas turbine engine in a humid environment. In test 1, first stage stator blades were made from AS800, and the engine was run for 815 hours. Test 4 was identical except the stator blade material was SN282, and the test ran for 1818 hours. Tests 2, 3, 5, and 6 are described in [2] with additional results given in Fig. 6 of [6]. These were conducted in the NASA high pressure burner rig (HPBR) using jet fuel in slightly lean equivalence ratios, for durations from 50 to 200 hours with AS800 and SN282 specimens.

Unfortunately, the resulting B_1 values do not agree very closely. To estimate recession rates in a way consistent with both series of tests, this mismatch must be reconciled.

Modified model

A minor change to the standard model yields much better agreement among values of B calculated from the engine and HPBR tests, as can be seen in the "B_2" column in Table 1. The proposed adjustment also resolves a theoretical error that emerged when the model was generalized beyond its underlying assumptions. Finally, it quantifies a phenomenon not explained by the standard model: in tests where the local variation in erosion rate is observable, the erosion rate is much higher than average at the leading edge of a specimen, and lower than average at the trailing edge.

The modified correlation is derived in the Appendix. It is suitable for a test sample or blade airfoil that can reasonably be approximated as a flat plate in laminar flow. The equations are:

$$\dot{y}_{l\_avg} = B_2 \frac{V^{0.5} P_{H2O}^2}{P_{total}^{0.5} L^{0.5}} \exp\left(\frac{-Q}{RT}\right) \quad (4)$$

$$\dot{y}_{l\_local} = \frac{B_2}{2} \frac{V^{0.5} P_{H2O}^2}{P_{total}^{0.5} x^{0.5}} \exp\left(\frac{-Q}{RT}\right) \quad (5)$$

[5] Rolls-Royce Allison, Indianapolis, IN

where

L is the specimen length in the streamwise direction (cm)

x is the distance downstream from the leading edge (cm)

$\dot{y}_{l\_avg}$ is the average recession rate (μm/hr)

$\dot{y}_{l\_local}$ is the local recession rate (μm/hr) at position x

B_2 is a new material constant (μm/hr) / [(m/s)$^{.5}$bar$^{1.5}$cm$^{-.5}$]

Table 1. Measured recession values and corresponding test conditions from published studies, and resulting "B_1" and "B_2" values. The boldface value is used in subsequent calculations.

#	Test	$\dot{y}_l$* $\frac{\mu m}{hr}$	V m/s	P_{H2O} bar**	P_{total} bar	L cm	T K	B_1 $\frac{\mu m/hr}{\left(\frac{m}{s}\right)^{.5} bar^{1.5}}$	B_2 $\frac{\mu m/hr}{\left(\frac{m/s}{cm}\right)^{.5} bar^{1.5}}$
AS800									
1	Engine	.748	573	.899	8.9	2.7	1561	474	780
2	HPBR	.242	20	.600	6	1.3	1600	1238	706
3	HPBR	.085	20	.600	6	1.3	1425	1178	672
SN282									
4	Engine	.380	573	.899	8.9	2.7	1533	280	**460**
5	HPBR	.097	20	.600	6	1.3	1499	855	474
6	HPBR	.079	20	.600	6	1.3	1473	812	450

* Recession rates reported by weight have been divided by an average density of 3.3 gm/cm^3 for Si_3N_4 to yield linear rates; thus 1 mg/cm^2/hr=3.03 μm/hr.

** Both references quote pressures in "atm" (normally 101,325 Pa) but appear to mean "bar" (100,000 Pa).

In the analyses that follow, we use a B_2 value of 460 (μm/hr)/[(m/s)$^{.5}$bar$^{1.5}$cm$^{-.5}$] to represent SN282. There is no commercial source for AS800 at present, and we do not have water vapor erosion data for other commercial silicon nitrides. We compute erosion rates at the trailing edge of the first stator blade row airfoils (by setting x=L and using equation (5)), because that is where erosion is the most damaging. Although erosion rates are higher at the leading edges, the velocity is much lower there, the flow is less sensitive to airfoil geometry, and the airfoils are much thicker. At the trailing edges, which are thin, there is little material to spare, and the trailing edge thickness affects the throat area and thus the blade row flow characteristic. Figure 6 in [9] shows an eroded blade after one of the engine tests, giving an idea of the relative magnitude of the problem at the leading vs. trailing edge. We assume an initial TE thickness of 0.8 mm and set 10% trailing edge thinning as the allowable maximum. Since recession occurs on both sides, this gives a limiting value of .04 mm, which is used in the life calculations below.

Having established a method for estimating the recession rate at the trailing edge of a ceramic rotor or stator blade, the next task is to estimate the water vapor content of the combustion products.

Water vapor content of combustion products

The best method of calculating the water vapor content of combustion products is to use a chemical equilibrium code, which models the high-temperature dissociation of combustion products into reactive radicals by Gibbs free energy minimization. This was done in [11], resulting in the following graph, which has been cited as justification for the assumption that water vapor content is about 10%.

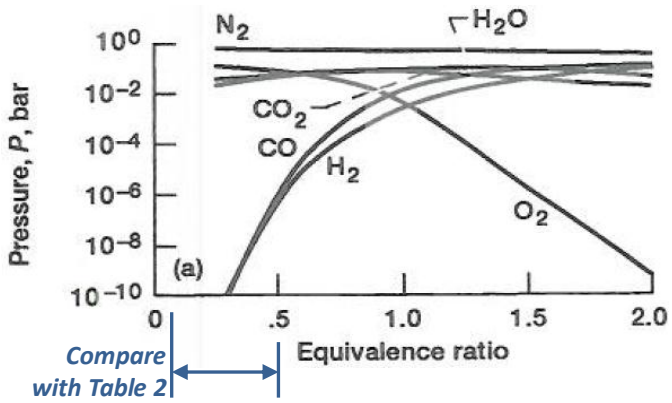

Figure 1. Reprinted from [11]: Equilibrium products of combustion for various *fuel-air* equivalence ratios Φ_{FA}. (Note, the remainder of this paper uses the *air-fuel* ratio: $\Phi_{AF}=1/\Phi_{FA}$.)

Though undisputed, this plot is difficult to read precisely due to the log scale; it does not provide results at lean enough air/fuel ratios for modeling recuperated cycles; and a computer program to calculate water vapor erosion requires an analytical model rather than a graph.

Alternatively, the water vapor content of combustion products can be estimated from a balanced chemical reaction equation (6), representing a hydrocarbon fuel C_xH_y burning in humid air (O_2 + 3.76N_2 + $n$$H_2O$). Jet-A fuel has a molar H:C ratio of about 1.92 [11] and is approximated as $C_{12}H_{23}$. Military fuels JP8 and JP5 are similar. Natural gas is typically ~95% methane [17] and is approximated here as CH_4.

The air-fuel equivalence ratio Φ_{AF} is the ratio of dry air to fuel (flow rates by mole or mass), divided by the stoichiometric ratio, per (7). The numerator of this expression is computed using a cycle model, provided later. The denominator, the dry stoichiometric air/fuel ratio, can be obtained from (6) by setting Φ_{AF}=1 and z=0, giving 84.5 mol/mol (14.6 gm/gm) for jet fuel and 9.52 mol/mol (17.1 gm/gm) for methane.

The number of moles of water vapor in the reactants, z, can be calculated from (8) along with assumed values for the relative humidity φ_{RH} and atmospheric pressure P_{atm} (bar). A fourth-order curve fit (9) gives the saturation pressure of water vapor in air, P_{sat} (bar), as a function of temperature T_{atm} (°C), from data points reported in [18].

Balanced reaction:

$$C_xH_y + (x+y/4)\Phi_{AF}O_2 + 3.76(x+y/4)\Phi_{AF}N_2 + zH_2O \rightarrow (x+y/4)(\Phi_{AF}-1)O_2 + xCO_2 + (y/2+z)H_2O + 3.76(x+y/4)\Phi_{AF}N_2 \quad (6)$$

Air-fuel equivalence ratio:

$$\Phi_{AF} \equiv \frac{\dot{m}_{air}/\dot{m}_{fuel}}{(\dot{m}_{air}/\dot{m}_{fuel})_{stoich}} \quad (7)$$

Moles of water vapor in reactants:

$$z = \frac{4.76\varphi_{RH}P_{sat}}{P_{atm} - \varphi_{RH}P_{sat}}(x + y/4)\Phi_{AF} \quad (8)$$

Water saturation pressure:

$$P_{sat} = 9.74\cdot10^{-9}T_{atm}^{4} - 3.54\cdot10^{-7}T_{atm}^{3} + 3.72\cdot10^{-5}T_{atm}^{2} + 1.43\cdot10^{-4}T_{atm} + 6.78\cdot10^{-3} \quad (9)$$

Concentration of water vapor in combustion products:

$$X_{H2O} = \frac{y/2 + z}{4.76\Phi_{AF}(x + y/4) + y/4 + z} \quad (10)$$

Even though the real chemistry is far more complex, these formulas are satisfactory for erosion calculations. This is demonstrated in Table 2, where the predictions of the balanced-reaction model are compared with output from the NASA equilibrium code used in [11].

Table 2. Equilibrium code output for 1700K, 1 atm products of fuel-lean Jet-A combustion in dry air. Species appearing in <1% concentrations (Ar, NO, CO, OH…) are omitted for brevity.

Equilibrium code						
Fuel/air eq. ratio Φ_{FA}	0.05	0.1	0.2	0.3	0.4	0.5
Air/fuel eq. ratio Φ_{AF}	20	10	5	3.33	2.5	2
[CO2], %	0.74	1.43	2.82	4.18	5.53	6.85
[H2O], %	0.65	1.31	2.63	3.93	5.22	6.49
[N2], %	77.5	77.2	76.7	76.2	75.7	75.2
[O2], %	19.5	18.4	16.2	14.1	11.9	9.86
Other species (Ar, NO, CO, OH, …) appear in concentrations below 1%.						
Current model						
[H2O] (X_{H2O}), %	0.68	1.35	2.69	4.00	5.30	6.58
Error	4.34%	3.13%	2.28%	1.83%	1.63%	1.45%

Clearly, for lean mixtures typical in turbine engines, the effects of dissociation are negligible. The mole fraction of water vapor is strongly dependent on the fuel-air ratio, and for dry air conditions and jet fuel, is always well below 10%. At other temperatures, pressures, and lean air-fuel ratios, the agreement between the two models remains good. Therefore, we advocate using the balanced-reaction model (6)-(9) in preference to either the overly simple 10% rule of thumb, or the overly complex equilibrium code method.

Next, we combine (4)-(9) with a thermodynamic model and some basic assumptions to predict water vapor erosion and cycle efficiency for a range of engine designs.

Cycle Model

Wilson ([19] pp. 103-106) provides formulas that allow the specific heat addition $\dot{Q}'$, specific work $\dot{W}'$, and thermal efficiency η_{th} to be calculated for both simple (CBE) and regenerative (CBEX) cycles. These are defined in (11)-(13). We assume the sum of all leakage flows equals the mass flow rate of fuel added in the combustor, so that the total mass flow of gas at any point in the engine is a constant: $\dot{m}_{burned\_gases} = \dot{m}_{air} + \dot{m}_{fuel} - \dot{m}_{leakage}$. The air/fuel equivalence ratio Φ_{AF} may be now be calculated from (14) for a particular compressor pressure ratio PR_c and turbine inlet temperature T_{ti}.

$$\dot{Q}' \equiv \frac{Heat\ addition}{\dot{m}_{air}\overline{Cp_c}T_{0,1}} = \frac{\dot{m}_{fuel}\,Q_{LHVfuel}}{\dot{m}_{air}\overline{Cp_c}T_{0,1}} \quad (11)$$

$$\dot{W}' \equiv \frac{Net\ power}{\dot{m}_{air}\overline{Cp_c}T_{0,1}} \quad (12)$$

$$\eta_{th} \equiv \frac{Net\ power\ out}{Net\ heat\ in} = \frac{\dot{W}'}{\dot{Q}'} \quad (13)$$

$$\Phi_{AF} = \frac{Q_{LHVfuel}}{\dot{Q}'\overline{Cp_c}T_{\mathrm{atm}}\,(\dot{m}_{air}/\dot{m}_{fuel})_{stoich}} \quad (14)$$

The following constants are assumed:

- Jet fuel lower heating value $Q_{LHVfuel}$=43.2MJ/kg
- Natural gas lower heating value $Q_{LHVfuel}$=47.1MJ/kg
- Atmospheric pressure P_{atm} = 1.00 bar at engine inlet
- Turbine polytropic efficiency η_{pt} = 80%
- Compressor polytropic efficiency η_{pc} = 85%
- Mean specific heat in compressor Cp_c = 1020 J/kg-K
- Mean specific heat in turbine Cp_t = 1230 J/kg-K
- Gas constant everywhere, R = 287 J/kg-K
- Burner pressure loss ΔP_b=5% of PR_c
- Heat exchanger air pressure loss ΔP_{hx_air}=.05 bar
- Heat exchanger exhaust pressure loss ΔP_{hx_ex}=.10 bar

We model heat exchanger pressure losses as constants, rather than scaling with the engine pressure ratio as is sometimes assumed. This gives overall cycle pressure losses 1-ΔP_b-$\Sigma\Delta P_{hx}$ = 1-PR_t/PR_c = 15.8% at PR_c=2, decreasing to 13.9% at PR_c=15, so it differs little from taking pressure losses as a fixed percentage. The present approach is simpler, and it reflects the greater difficulty of designing a low-loss heat exchanger for low pressure ratio, low specific work engines with their larger gas flow rates per unit power output.

Mean Blade and Gas Speeds

To analyze water vapor erosion rates also requires the local gas velocity. Mean blade and gas speeds at the first stator trailing edge depend on PR_c, T_{ti}, the number of turbine stages, and their efficiencies and velocity diagrams (work, flow, and reaction coefficients). It is always possible to reduce blade and gas velocities by using more turbine stages. Doing this improves efficiency and reduces stresses, but also increases weight and complexity. Thus there is a tradeoff to be made.

A central point of this paper is that when ceramic turbine life and reliability are important, it helps to keep blade speeds well below the typical 500-600 m/s range. Here the blade speed is limited to 350 m/s by adjusting the number of stages, N_{st}. At the lowest pressure ratios, two turbine stages are retained even if the blade speed could be held below the limit

with only one stage. This was done because it shows that blade speeds as low as 260 m/s are quite practical in low pressure ratio engines. Commercial engines sometimes use two stages even when one would suffice, to give the flexibility of a two-shaft engine with a free power turbine. With cantilever-supported turbine rotors, there is no need for concentric shafts, and the bearings can all be located away from the hot section components. This common layout retains most of the simplicity and cost advantages of a single-stage engine [20].

In the tables that follow, it is assumed that each stage operates at a work coefficient Ψ=2.0, a flow coefficient φ=0.6, and a degree of reaction Rn=50%. Relative blade speeds, gas speeds, and Mach numbers are calculated as follows:

Turbine pressure ratio $PR_t = 1 + (PR_c\text{-}1)(1\text{-}\Sigma\Delta P_0)$

Turbine temperature ratio $TR_t = PR_t\text{^}(R\eta_p/Cp_t)$

Turbine total enthalpy change $\Delta h_{0t} = Cp_t T_{ti}(1\text{-}\ 1/TR_t)$

Stage blade speed $u = \sqrt{\Delta h_{0t}/(\Psi \cdot N_{stages})}$

Relative gas velocity $C_{TE} = u\sqrt{(1 - Rn + \Psi/2)^2 + \varphi^2}$

Ratio of specific heats $\gamma_t = Cp_t / (Cp_t\text{-}R)$

Trailing edge Mach number $M_{TE} = \frac{C_{TE}}{\sqrt{\gamma_t R T_{ti}}}$

Results and Discussion

Table 3 gives results for T_{ti}=1200°C in engines burning jet fuel and operating in ambient conditions of 15°C and 50% relative humidity.

Observations:

- The exhaust water vapor content is below 10% in all cases, and is especially low in recuperated engines.
- The high air-fuel ratios in low-PR_c recuperated engines result in very low water vapor contents, and hence much longer turbine lives. For example, at PR_c=3, the recuperated engine lasts over 10,000 hours, almost six times as long as the simple cycle engine.
- All life estimates are in the hundreds of hours, indicating that short-life engines for missiles or expendable UAVs, whether recuperated or not, could use ceramic turbines.
- A two-stage turbine can operate at blade speeds below 350 m/s, for pressure ratios up to about 5:1.

Table 4 shows how the burned gas water vapor content varies depending on fuel type and turbine inlet temperature, and quantifies the effect of ambient humidity. Aircraft and missiles mostly operate at altitudes, where the air is dry, so standard-day conditions (T=15°C, φ_{RH}=50%) represent a conservative assumption. However, for applications like stationary power generation in humid climates, an engine may operate in high humidity for its entire life. Here we use the average dew point in Bangkok, Thailand [21], one of the most humid climates in the world, to represent worst-case conditions.

Table 3. Number of turbine stages, blade speeds, relative gas speeds and Mach numbers, fuel/air ratios, burned gas water vapor contents, erosion rates, and turbine life for T_{ti}=1200°C, 2cm blade chord, Jet-A fuel, standard day (15°C, φ_{RH}=50%).

PR_c	PR_t	P_{ti} bar	N_{st}	u m/s	C_{TE} m/s	M_{TE}	Φ_{AF}	X_{H2O}	$\dot{y}_l$ μm/hr	Life hr
Simple Cycle										
2	1.90	1.90	2	226	365	.492	2.17	6.8%	.0113	3,553
3	2.85	2.85	2	284	458	.617	2.28	6.6%	.0213	1,874
5	4.75	4.75	2	338	546	.736	2.45	6.2%	.0442	905
7	6.65	6.65	3	300	485	.653	2.61	5.9%	.0623	642
10	9.50	9.50	3	322	520	.700	2.82	5.5%	.0968	413
15	14.25	14.25	3	344	555	.748	3.14	5.0%	.1535	261
Recuperated Cycle										
2	1.68	1.85	2	205	331	.446	8.53	2.4%	.0013	31,630
3	2.55	2.80	2	269	435	.586	6.71	2.8%	.0037	10,731
5	4.28	4.70	2	328	530	.714	5.42	3.3%	.0121	3,294
7	6.00	6.60	3	293	473	.637	4.87	3.6%	.0224	1,787
10	8.59	9.45	3	316	511	.688	4.44	3.8%	.0458	873
15	12.91	14.20	3	339	547	.737	4.08	4.1%	.0997	401

Table 4. Burned gas water vapor content (mol%) for various pressure ratios, turbine inlet temperatures, fuels, and standard (15°C, φ_{RH}=50%) vs. humid (23°C, φ_{RH}=100%) conditions.

PR_c	Jet Fuel						Natural Gas					
	Standard Day			Humid Day			Standard Day			Humid Day		
	1050°	1200°	1350°	1050°	1200°	1350°	1050°	1200°	1350°	1050°	1200°	1350°
Simple Cycle												
2	6.0	6.8	7.6	7.8	8.6	9.3	9.4	10.6	11.9	11.0	12.2	13.4
5	5.4	6.2	6.9	7.1	7.9	8.7	8.3	9.5	10.8	9.9	11.1	12.4
15	4.2	5.0	5.8	6.0	6.7	7.5	6.4	7.7	9.0	8.0	9.3	10.5
Recuperated Cycle												
2	2.2	2.4	2.6	4.1	4.3	4.5	3.1	3.4	3.7	5.0	5.3	5.6
5	3.0	3.3	3.6	4.9	5.1	5.4	4.4	4.9	5.3	6.2	6.7	7.1
15	3.7	4.1	4.5	5.5	5.9	6.3	5.5	6.2	6.8	7.3	7.9	8.5

Burned gas water vapor contents vary greatly, from near 2% in low-PR_c recuperated engines on jet fuel in standard conditions to over 13% for low-PR_c simple cycle engines in humid climates on natural gas. Since water vapor partial pressure is *squared* in the erosion rate model, H_2O content and pressure ratio variations lead to tremendous variability in turbine life, especially at high turbine inlet temperatures, as shown in Table 5 and Figure 2. Some noteworthy trends:

- Humid conditions reduce the turbine life in simple cycle engines by a factor of 1.5-2, and in recuperated engines by a factor of 2-3. In the latter, leaner air-fuel ratios produce less water in the exhaust, so humidity plays a bigger role.
- The change from jet fuel to natural gas reduces engine life by roughly a factor of two in all cases, reflecting the higher H:C ratio of CH_4 vs. $C_{12}H_{23}$.

- Nevertheless, in recuperated engines, turbines without environmental barrier coatings can last for thousands of hours – even in humid climates on natural gas fuel.

Table 5. Erosion-limited life (hr) for 1200°C turbine inlet temp. for jet fuel vs. natural gas, and standard vs. humid conditions.

PR_c	Simple Cycle				Recuperated Cycle			
	Jet fuel		Natural gas		Jet fuel		Natural gas	
	Std	Hum	Std	Hum	Std	Hum	Std	Hum
2	3,553	2,265	1,471	1,113	31,630	9,855	15,512	6,505
3	1,874	1,175	778	582	10,731	3,854	5,033	2,402
5	905	552	377	277	3,294	1,338	1,492	792
7	642	383	269	194	1,787	770	797	445
10	413	239	174	123	873	396	385	224
15	261	144	111	76	401	190	175	106

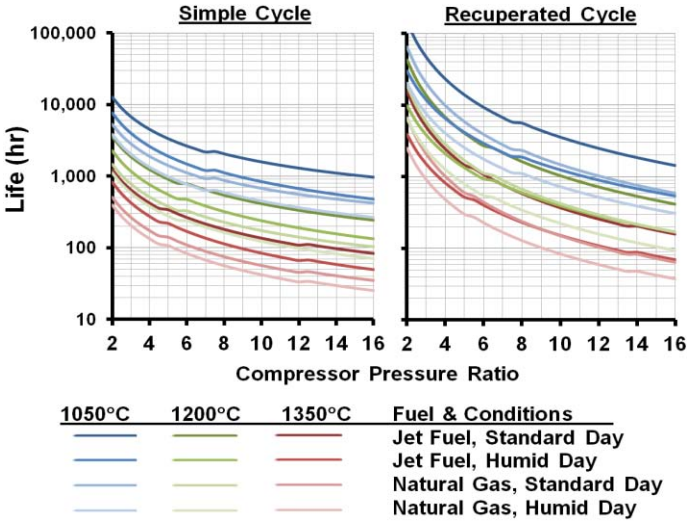

Figure 2. Data from Table **5**, with lower (1050°C) and higher (1350°C) turbine inlet temperatures for comparison. Bumps in curves reflect increments in number of turbine stages to keep blade speeds

In conclusion, in this section we have provided a revised water vapor erosion model and a precise way to estimate the water vapor content in burned gases. We have used these tools along with a cycle model based on small-engine component efficiencies, to quantify the water erosion rates for various engine types. These included simple and recuperated turbines operating at various pressure ratios and turbine inlet temperatures, in standard and humid atmospheres, on two different fuels. The results show that ceramic turbines will last hundreds of hours in almost any engine type; thousands of hours in low pressure ratio engines, whether simple or recuperated; and tens of thousands of hours in low pressure ratio recuperated engines.

We have also demonstrated that in the latter type of engine, extremely low blade speeds (220-350 m/s) and relative gas Mach numbers (.50-.75) can be used in engine configurations that are nevertheless simple and practical. Later in this paper, we also show that they are highly efficient. In the upcoming sections, we examine whether low blade speeds could be an effective design strategy for circumventing several other stumbling blocks for ceramic turbines: slow crack growth, foreign object damage, and perhaps even cost.

SLOW CRACK GROWTH

To quantify the beneficial effects of low blade speeds on reliability, the CARES/*Life* integrated design code [22] has been used to assess the probability of failure due to fast fracture and slow crack growth (SCG), for an example turbine rotor. The radius at the blade midspan is 25 mm, resulting in a mean blade speed of 262 m/s at 100,000 rpm. Details on the example rotor and the engine for which it was designed are in [20]. The analysis that was conducted is described in [23, 24], from which much of the material in this section was taken.

CARES/Life

Randomly-distributed internal and surface flaws in brittle materials cause their apparent strength to vary from specimen to specimen, even under identical testing conditions. CARES/*Life* predicts the failure probability of a ceramic component by combining finite element analysis with stochastic information about the material strength [25, 26]. The latter is determined from rupture testing of nominally identical specimens in simple tension or flexure, using regression techniques. The probabilistic nature of material strength is modeled by the Weibull cumulative distribution function [27].

For uniaxially stressed components, the two-parameter Weibull distribution for volume flaws describes the *fast-fracture* failure probability, P_f, as

$$P_f = 1 - exp\left[-\frac{1}{{\sigma_{0V}}^m}\int_V \sigma(x,y,z)^m dV\right] \quad (15)$$

where V is the volume, $\sigma(x,y,z)$ is the uniaxial stress at a point location in the body, and m and σ_{0V} are the shape and scale parameters of the Weibull distribution, with σ_{0V} given in units of stress·volume$^{1/m}$. An analogous equation based on surface area can be derived for surface flaws. To predict reliability for multiaxial stress states, the Principle of Independent Action (PIA) theory [28] or Batdorf theory [29] is used. Batdorf theory combines the weakest link theory with linear elastic fracture mechanics. It includes the calculation of the combined probability of the critical flaw being within a certain size range and being located and oriented so that it may cause fracture.

Slow crack growth refers to the stable extension of a crack over time. It results from the combination of stress at the crack tip and chemical attack, such that chemical bonds break and the crack tip extends. The crack length, a, as a function of time, t, can be expressed as a power law [30] of the form

$$\frac{da}{dt} = A \cdot {K_{I_{eq}}}^N \quad (16)$$

where K_{Ieq} is the equivalent mode I stress intensity factor from the applied effective stress, and A and N are material parameters that depend on the temperature and environment. A and N thus vary with position and time, while a and K_{Ieq} are functions of position, time, and crack orientation. CARES/*Life* tracks these variations, takes into account the time dependence of loading and material response, and integrates the results from all elements to evaluate the overall component reliability.

Example Rotor Properties and Loads

To shed light on the relative importance of centrifugal vs. thermal stresses, two studies were conducted. The first was based on structural loading alone, while the second also included transient thermal effects. Due to software limitations, both studies focused only on volume-based flaws. Several materials were considered: two turbine-grade silicon nitrides, and a zirconia-toughened mullite (ZTM) composite under study at NRL. Their properties are shown in Table 6 and Table 7. The ZTM material properties are developmental goals only, and have *not* been achieved or even measured yet.

Table 6. Mechanical and physical properties for the considered ceramic materials.

Material	Elastic modulus GPa	Poisson's ratio	Density kg/m^3	CTE μm/m·K	Specific heat J/kg·K	Thermal conduct. W/m·K
SN282	305	0.28	3380	2.9	1200	30
NT154	310	0.27	3230	2.9	1100	30
Mullite*	150	0.24	2800	5.3	950	8

*Zirconia-toughened mullite composite being developed at NRL

Table 7. Weibull and SCG parameters for the considered ceramic materials. The parameters were calculated using scaled bending strength from tensile strength data.

Material	Weibull modulus m	Characteristic strength σ_θ, MPa	Volume scale parameter σ_{0V}, MPa·mm$^{3/m}$	SCG exponent N	SCG coeff. B_V, MPa·sec
SN282	30	540	570	105	2,053
NT154	7.5	670	970	17	146,000
Mullite**	15	390	445	25	15,700

**Properties listed here are estimates or development goals, not measurements

The second analysis included centrifugal stress due to 100,000 rpm rotation, and thermal stress due to sudden heating when the burner was lit. With the rotor initially at 15°C, a convection boundary condition was applied to exposed surfaces as shown in Figure 3, with a heat transfer coefficient of h=627 W/m^{2}K and a gas temperature of 1225°C. The duration of a "load block" was 10 minutes. After each load block, the stress and thermal states were reset, and another block began, with damage accumulating.

Figure 3. Surfaces where convection condition was applied (h=627 W/m^{2}K, 1225°C). Initial rotor temperature was 15°C. The diameter at the blade tips is 58 mm.

It should be borne in mind that this rotor design is fairly conventional, and much has already been done to minimize all types of stresses. For example, the blades are stacked radially; the airfoils are much thicker at the root than at the tip; blade root fillets are as large as possible to minimize the stress concentration there; the hub has a nearly ideal radial thickness distribution; and the hub center is solid (no bore), which reduces hub stresses by 50%. Thermal stresses are presumably lower for the present design than for a radial-flow rotor of equal size, due to the higher mass and thermal inertia of the hub in the latter case; and should be much better than large rotors of either axial or radial flow design, due to the thermal uniformity that results from simply being small.

With this in mind, we move on to presenting results from both studies to show the beneficial effects of low blade speeds.

Results

Table 8 shows the results of purely centrifugal loading, when the rotor is made from SN282. The ANSYS model predicted a maximum principal stress of 101 MPa at 100,000 rpm.

Table 8. Probability of failure due to fast fracture and slow crack growth, for SN282 material and various speeds. 100,000 rpm equals 262 m/s mean blade speed.

Speed rpm	Probability of failure, P_f				
	Fast fracture	1 day	1 month	1 year	10 years
100,000	0.00E+00	0.00E+00	0.00E+00	0.00E+00	0.00E+00
120,000	1.11E-16	4.11E-15	1.10E-14	2.29E-14	4.49E-14
140,000	9.74E-13	5.09E-11	1.37E-10	2.85E-10	5.58E-10
160,000	2.94E-09	1.79E-07	4.84E-07	1.00E-06	1.97E-06
180,000	3.44E-06	2.41E-04	6.51E-04	1.35E-03	2.64E-03
200,000	1.91E-03	1.41E-01	3.36E-01	5.73E-01	8.11E-01
210,000	3.52E-02	9.50E-01	1.00E+00		
232,500	1.00E+00				

It is easy to see how a turbine designer could be lulled into a false sense of security if thermal stresses (which are labor-intensive to simulate) are ignored. At the design speed of 100,000 rpm, the probability of failure is zero. When *only*

thermal stresses were considered, the stress peaked at 172 MPa but then fell to an equilibrium level of only 53 MPa [24] after about 100 seconds. Figure 4 shows the time history of combined centrifugal and transient thermal loads during each load block. The final stress is 339 MPa.

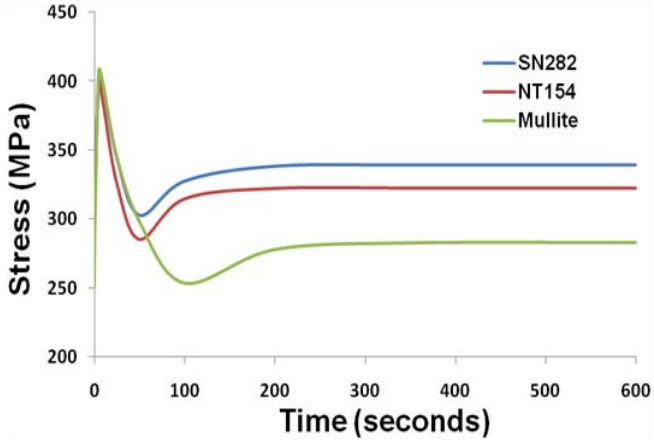

Figure 4. Thermal+centrifugal stress for the example rotor, for SN282, NT154, and mullite composite material.

Table 9 provides the resulting probability of failure due to slow crack growth, and also includes results from the studies when the material was NT154 or ZTM.

Table 9. Reliability analysis results based on combined transient thermal and centrifugal loads at 100,000 rpm.

# load blocks	Time (sec)	Probability of failure due to SCG		
		SN282	NT154	Mullite
1	10 min	1.22E-04	1.49E-01	0.9999
10	100 min	2.38E-04	3.68E-01	1.0
100	16.7 hrs	4.66E-04	7.62E-01	1.0
144	1 day	5.18E-04	8.21E-01	1.0
4320	1 month	1.40E-03	1.00E+00	1.0
51840	1 year	2.89E-03	1.00E+00	1.0
518400	10 years	5.64E-03	1.00E+00	1.0

Discussion

From the foregoing, several conclusions can be drawn. First, thermal stresses – both transient and steady - are much greater than centrifugal stresses, for the design analyzed here (>400 MPa transient vs. 340 MPa steady). Other integrally bladed rotors have behaved similarly, e.g. [31]. It seems likely that most rotors of conventional design will have similar transient thermal stress distributions unless special measures are taken. Special measures could include non-blisk designs, for example individual blades mounted to the hub with compliant elements, or a starting procedure designed to minimize thermal shock.

Second, it is interesting that this analysis suggests combined thermal and centrifugal stresses will be so high. The first analysis (centrifugal loads only) gives 110 MPa steady stress, while the steady centrifugal+thermal stress is 340 MPa. This is presumably due to the fact that a 15 deg. C temperature boundary condition was imposed at the end of the protruding shaft, where it mates with the well-cooled metal bearing shaft assembly. This heat sink keeps the center of the hub cool relative to the rim, resulting in compressive stresses at the rim which exacerbate the blade root stresses greatly. This has been corroborated by an FEA analysis in a different software package with the same rotor shape and boundary conditions.

This leads to the third conclusion, which is that integrally bladed disks, while ideal from a cost and simplicity point of view, are at risk from thermal stresses. One avenue for exploration may be to add short meridional cuts in the hub rim between each pair of blades, dividing the rim into segments that are free to expand and contract with temperature.

Fourth, despite the thermal stress issue, the analysis above suggests that the present design will achieve more than adequate reliability, at least from a SCG standpoint, for its application. The rotor is predicted to have 99.95% reliability after 4320 hours, including 144 start/stop cycles, despite the relatively high thermal stresses predicted.

Fifth, if the rotor had been designed for a more typical blade speed – about 550 m/s – then the steady stress due *only* to centrifugal loads would have been 3-4 times the present level. This would correspond to the 200,000 rpm case. Here the probability of failure is much higher: Pf=34% after 4320 hours (one month) and 144 start/stop cycles.

Thus it is clear that for the present rotor design, low blade speeds are not only advantageous, they are essential. Since the present rotor design is quite conventional, by extension the same conclusion may be extended to all ceramic turbine rotors, with the possible exception of novel designs with features that somehow keep combined centrifugal and transient thermal stresses in the ~300 MPa range despite higher blade speeds.

FOREIGN OBJECT DAMAGE

The effects of FOD impact on ceramic turbine materials have been studied extensively [13-16, 32]. Many studies have identified a "critical impact velocity", below which particles of a given mass that impact a substrate of specific dimensions may cause no damage at all. For example, standard 3x4x45mm flexure bars were subjected to hardened steel balls at various impact velocity by Choi et al [13], who found essentially no damage or loss of strength at impact velocities below 300 m/s for SN282 specimens, and 400 m/s for AS800.

The above conclusion was drawn only for impact targets in the shape of standard bend bars, 3mm thick. Thinner targets have since been shown to be significantly more vulnerable to FOD damage when the particle size was the same (1.6 mm diameter steel or silicon nitride balls). The example rotor used in the SCG analysis above has blades that are at most 1.5mm thick, so if an object with the mass of a 1.6mm steel ball were to impact it, they would surely be damaged.

On the other hand, smaller engines are less likely to ingest large particles than larger engines. The 1.6mm steel ball

discussed above would barely fit between two of the blades of the sample rotor described above. Thus this size particle is a boulder relative to the example rotor, but a pebble relative to a large engine such as the Rolls-Royce model 501-K engine discussed in the water vapor section below. The latter had stator blades of 27mm chord, and judging from the profile drawn in [8], a maximum thickness around 3mm.

Furthermore, for shaft power engines, it should be possible to reduce the probability of foreign object damage by placing an air filter upstream from the compressor inlet. In this case, assuming no foreign objects of mass greater than the damaging kinetic energy threshold are present in the engine before the air filter is attached, the risk of FOD is mainly due to particles generated in the engine during operation. Most often these consist of some form of carbon deposit, with hardness and density below that of steel, so that the probability of damage should be lower.

In summary, the relative velocity of particles impacting the turbine rotor blades will likely be less than or equal to the blade speed. Thus, limiting blade speeds to about 350 m/s should greatly improve reliability and life. In the special case of shaft power engines designed for land-based use, where the weight of a large air filter is tolerable, this approach may be used in combination with the low blade speed strategy to keep the risk of foreign object damage within tolerable limits.

Finally, it is worth noting that reference [13] shows critical impact velocities for environmental barrier coatings on similar specimens with the same steel balls were much lower: 100-200 m/s. It was shown in the water vapor erosion section that uncoated turbines can last thousands of hours in recuperated engine designs. Eliminating the EBC may also be a significant cost advantage. Therefore, in low pressure ratio recuperated engines, avoiding the use of EBCs is an approach worth considering.

COST

A final obstacle for ceramic turbines is cost. The same obstacle prevented metal gas turbines from being used in the automotive market [33]. However, for decades, ceramic turbocharger rotors have been produced at rates exceeding 10,000 per month by Kyocera and others, for the notoriously cost-sensitive automotive market [34]. For guidance on desigining low-cost ceramic components, we therefore turn to a cost study by Kyocera [35] for a ceramic turbine stator.

The lesson from this study is that diamond grinding is by far the most expensive step in the production of ceramic parts. Further conversations with this manufacturer revealed that grinding exterior surfaces of parts, where there is room to use a large grinding wheel, is not a costly process because material removal rates are high. An example is the blade tip OD of the example rotor. Conversely, using small-diameter diamond bits to grind hard-to-reach interior areas such as the blade airfoil surfaces is a slow and very time consuming process.

When the Mach number of the flow over the blades is relatively low, the flow is relatively insensitive to small flaws or geometric imperfections in the blade surfaces. Also, the trailing edge drag is lower, improving efficiency or allowing the trailing edges to be thicker, reducing their tendency to chip. The latter would tend to improve part yield and thus reduce costs. Finally, due to lower stresses, the final inspection cost could be far lower, since expensive steps such as proof-testing, computed tomography, or x-ray inspection could be eliminated. As a result, in the case of the example rotor, it was estimated that in high-rate production via the green-machining process, the primary factor controlling the cost would be the raw materials. We mention these facts as evidence that lower blade speeds could lead to significantly lower production costs for ceramic turbines.

Thus far we have shown, hopefully, that the reliability, life, and cost of ceramic turbines can be improved through careful selection of the thermodynamic cycle, and through the use of lower blade speeds. The final question is whether the engine designs that result from actually using these two strategies could present an attractive business case; and, if so, in what markets? This is the topic for the next section.

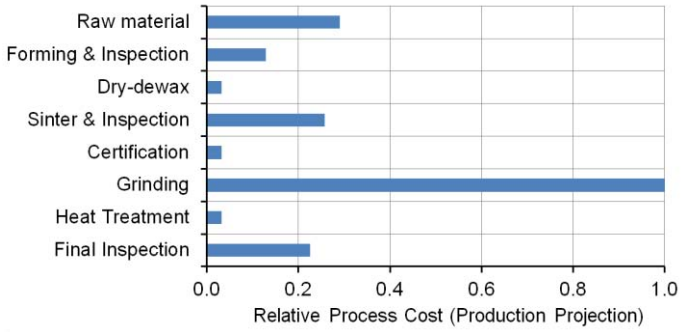

Figure 5. Estimated relative production cost of various stages in the process of manufacturing a ceramic turbine component, taken from a Kyocera cost study referenced in [35].

MARKET IMPLICATIONS

We may use the same cycle model developed in the Water Vapor Erosion section to shed light on the important question of suitable target markets. As a roadmap, Table 10 provides life, efficiency, and specific work calculations for various temperatures and pressure ratios, based on standard-day humidity and jet fuel.

For markets in which *moderate* lives in the 1,000-4,000 hour range are acceptable, the table shows that recuperated ceramic gas turbines could deliver exceptionally high fuel efficiencies. One particularly attractive design point is the 5:1 pressure ratio, 1200C turbine inlet temperature recuperated cycle. It has a reasonably long engine life (~3300 hours) and an extremely high cycle efficiency of 41%, giving a specific fuel consumption of 203 gm/kW-hr (.334 lb/hp-hr). Small to medium size piston engines, even diesels, would struggle to match this. Thus, this type of engine could be used for unmanned air vehicles, backup power generation, military portable power, general aviation, RV and boat power

generation, general aviation, and perhaps even automotive markets. The foregoing are listed in increasing order of increasingly challenging production cost requirements.

When recuperation absolutely must be avoided, but turbine life still matters, moderate lives in the 1,000-2,000 hour range can be achieved along with moderate efficiencies, but only by reverting to the 1050°C column. Although metal turbines could also operate at this temperature, perhaps in some applications the creep resistance and low density of ceramics may make them worth considering anyway. Simple cycle engines with ceramic turbines might also make sense in moderate-life applications where the engine operates on jet fuel, in medium-to-low ambient humidity, and at max rated temperature for only a small portion of its life. For example, consider a UAV engine designed to run at maximum power (PR_c=10, T_{ti}=1350°C) for a 20-minute climb-out, then at cruise power (perhaps PR_c=5, T_{ti}=1050°C) for the remainder of a 12-hour flight. A weighted average gives a life estimate of 1684 hours for this case, with the engine operating at 20% efficiency (SFC = 417 gm/kW-hr or .69 lb/hp-hr) or better throughout the flight.

On the other end of the spectrum, ceramic turbines and extremely high degrees of recuperation (ε_{hx}>95%) could be used for stationary power generation, even on natural gas in humid climates. Wilson has observed that even sub-megawatt generators of this type could reach efficiencies well above 50% [19, 36]. Some illuminating treatises on this subject, and on other target markets for ceramic and recuperated/regenerated turbines are provided in [37-42]

Table 10. Efficiency and specific work for various engine cycles based on jet fuel, 15°C, and 50% humidity. Conservatively, one can divide life by 2 for natural gas, 3 for humid weather, or 6 for both. Efficiency and specific work are unaffected.

PR_c	Life (hr)			Efficiency			Specific Work		
	1050°	1200°	1350°	1050°	1200°	1350°	1050°	1200°	1350°
Simple Cycle									
2	12,683	3,553	1,236	9%	9%	10%	.37	.44	.51
3	6,767	1,874	646	14%	15%	15%	.55	.66	.77
5	3,333	905	340	20%	21%	21%	.69	.85	1.01
7	2,173	642	215	23%	24%	25%	.75	.93	1.12
10	1,581	413	136	26%	27%	28%	.76	.97	1.19
15	1,032	261	90	28%	30%	31%	.72	.96	1.21
Recuperated Cycle									
2	104,057	31,630	11,745	25%	27%	28%	.26	.31	.37
3	35,667	10,731	3,951	34%	37%	39%	.45	.55	.65
5	11,048	3,294	1,203	37%	41%	44%	.61	.76	.91
7	5,443	1,787	650	37%	41%	44%	.67	.85	1.03
10	2,955	873	316	34%	39%	43%	.69	.90	1.10
15	1,365	401	156	30%	36%	41%	.65	.89	1.13

CONCLUSIONS

Two design strategies are very helpful for improving the life and reliability of uncoated ceramic turbines: the use of recuperated cycles and low pressure ratios to reduce water vapor erosion, and the use of very low mean blade speeds to reduce slow crack growth and foreign object damage.

Recuperated engines operate at lean air/fuel ratios, produce less water vapor in the exhaust, and reach peak efficiency at low pressure ratios. Together, these factors greatly reduce erosion rates, yielding lives exceeding 10,000 hours in very practical design scenarios, even without EBCs.

Two improvements to standard methods for forecasting water vapor erosion rates have been proposed in this paper. One is an adjustment to the basic equation to bring it into agreement with the flat plate mass transfer correlation from which it was derived. The other is to recognize that the air/fuel ratio, fuel type, and ambient humidity all significantly influence the burned gas water vapor content, and hence the water vapor erosion rate. It is not adequate to model the water vapor content of the burned gases as fixed at 10%. Simple formulas have been provided, enabling all relevant variables to be computed in a simple spreadsheet-type model, for any engine design and environment.

Unusually low mean blade speeds in the 220-350 m/s neighborhood can result in extremely high reliability levels, even for simple integral bladed disk designs with significant transient thermal stresses and very aggressive thermal cycling schedules. For various reasons, lower blade speeds could lead to significantly lower production costs for ceramic turbines. Finally, foreign object damage vulnerability is dramatically reduced by the use of such low blade speeds.

In long-life, high-efficiency recuperated engines designed for low blade speeds and pressure ratios, ceramic turbines are ready for application today.

ACKNOWLEDGEMENTS

Support for this work was provided by the Naval Research Lab 6.2 Base program, and is gratefully acknowledged.

BIBLIOGRAPHY

[1] Richerson, D. W., 2006, "Historical review of addressing the challenges of use of ceramic components in gas turbine engines," Proceedings of the ASME Turbo Expo 2006, Vol 2, pp. 241-254.

[2] Smialek, J. L., Robinson, R. C., Opila, E. J., Fox, D. S., and Jacobson, N. S., 1999, "SiC and Si3N4 recession due to SiO2 scale volatility under combustor conditions," Advanced Composite Materials, 8(1), p. 33.

[3] Opila, E. J., 2003, "Oxidation and Volatilization of Silica Formers in Water Vapor," Journal of the American Ceramic Society, 86(8), pp. 1238-1248.

[4] Jacobson, N. S., Opila, E. J., and Lee, K. N., 2001, "Oxidation and corrosion of ceramics and ceramic matrix composites," Current Opinion in Solid State and Materials Science, 5(4), pp. 301-309.

[5] Fox, D. S., Opila, E. J., Nguyen, Q. N., Humphrey, D. L., and Lewton, S. M., 2003, "Paralinear oxidation of silicon nitride in a water-vapor/oxygen environment," Journal of the American Ceramic Society, 86(8), pp. 1256-1261.

[6] Opila, E. J., Robinson, R. C., Fox, D. S., Wenglarz, R. A., and Ferber, M. K., 2003, "Additive Effects on Si3N4

Oxidation/Volatilization in Water Vapor," Journal of the American Ceramic Society, 86(8), pp. 1262-1271.
[7] Lin, H. T., and Ferber, M. K., 2002, "Mechanical reliability evaluation of silicon nitride ceramic components after exposure in industrial gas turbines," Journal of the European Ceramic Society, 22(14-15), pp. 2789-2797.
[8] Lin, H.-T., Ferber, M. K., Westphal, W., and Macri, F., 2002, "Evaluation of Mechanical Reliability of Silicon Nitride Vanes After Field Tests in an Industrial Gas Turbine," ASME Conference Proceedings, 2002(36096), pp. 147-154.
[9] Ferber, M. K., Lin, H. T., Parathasarathy, V., and Wenglarz, R. A., "Degradation of Silicon Nitrides in High Pressure, Moisture Rich Environments," Proc. IGTI Turbo Expo 2000, ASME.
[10] Ferber, M. K., 2005, "International Energy Agency Implementing Agreement for a Programme of Research and Development on Advanced Materials for Transportation Applications, Annex II: Co-Operative Program on Ceramics for Advanced Engines and Other Conservation Applications; Burner Rig Round Robin - Subtask 13 Final Report," Oak Ridge National Laboratory.
[11] Jacobson, N. S., 1993, "Corrosion of Silicon-Based Ceramics in Combustion Environments," Journal of the American Ceramic Society, 76(1), pp. 3-28.
[12] Jacobson, N., Myers, D., Opila, E., and Copland, E., 2005, "Interactions of water vapor with oxides at elevated temperatures," Journal of Physics and Chemistry of Solids, 66(2-4), pp. 471-478.
[13] Choi, S. R., Pereira, J. M., Janosik, L. A., and Bhatt, R. T., 2004, "Foreign object damage in flexure bars of two gas-turbine grade silicon nitrides," Materials Science and Engineering: A, 379(1-2), pp. 411-419.
[14] Choi, S. R., 2009, "Foreign Object Damage in Gas-Turbine Grade Silicon Nitrides by Silicon Nitride Ball Projectiles," ASME Conference Proceedings, 2009(48821), pp. 241-248.
[15] Choi, S. R., Pereira, J. M., Janosik, L. A., and Bhatt, R. T., 2003, "Foreign Object Damage of Two Gas-Turbine Grade Silicon Nitrides in a Thin Disk Configuration," ASME Conference Proceedings, 2003(36843), pp. 597-606.
[16] Choi, S. R., Racz, Z., Bhatt, R. T., Brewer, D. N., and Gyekenyesi, J. P., 2005, "Effect of Projectile Materials on Foreign Object Damage of a Gas-Turbine Grade Silicon Nitride," ASME Conference Proceedings, 2005(46997), pp. 339-349.
[17] "Chemical Composition of Natural Gas," web site, http://www.uniongas.com/aboutus/aboutng/composition.asp.
[18] Moran, M. J., and Shapiro, H.N., 1988, Fundamentals of Engineering Thermodynamics, 2nd Ed., John Wiley & Sons, New York.
[19] Wilson, D. G., and Korakianitis, T., 1998, The Design of High-Efficiency Turbomachinery and Gas Turbines, Prentice-Hall, Upper Saddle River, NJ.
[20] Vick, M. J., Heyes, A., and Pullen, K., 2010, "Design Overview of a Three Kilowatt Recuperated Ceramic Turboshaft Engine," Journal of Engineering for Gas Turbines and Power, 132(9), p. 092301.
[21] "Almanac: Historical Weather Information for Bangkok, Thailand," www.myforecast.com.
[22] CARES/*Life* v. 9.0, Connecticut Reserve Technologies, Inc., Gates Mills, OH.
[23] Wereszczak, A. A., and Jadaan, O., 2009, "Reliability Analyses for the NRL Ceramic Rotor, Part I: Centrifugal Load," Oak Ridge National Laboratory.
[24] Wereszczak, A. A., and Jadaan, O., 2009, "Reliability Analyses for the NRL Ceramic Rotor, Part II: Transient Thermomechanical Load ".
[25] Nemeth, N. N., Jadaan, O. M., and Gyekenyesi, J. P., 2005, "Lifetime Reliability Prediction of Ceramic Structures under Transient Thermomechanical Loads."
[26] Nemeth, N. N., Jadaan, O. M., Baker, E. H., and Gyekenyesi, J. P., "Lifetime Reliability Prediction of Ceramics Subjected to Thermal and Mechanical Cyclic Loads", ASME Turbo Expo 2007, GT2007-27047, May 14-17, 2007, Montreal, Canada.
[27] Weibull, W. A., 1939, "A Statistical Theory of the Strength of Materials," No. 151, Ingenoirs Vetenskaps Akadanien Handlinger.
[28] Freudenthal, A. M., 1968, "Statistical Approach to Brittle Fracture," Fracture, An Advanced Treatise, H. Liebowitz, ed., Academic Press, New York, N.Y., pp. 591-619.
[29] Batdorf, S. B., and Heinisch, H. L., Jr., 1978, "Weakest Link Theory Reformulated for Arbitrary Fracture Criterion," Journal of the American Ceramic Society, 61(7-8), pp. 355-358.
[30] Wiederhorn, S. M., 1974, "Subcritical Crack Growth in Ceram¬ics," Fracture Mechanics of Ceramics, R. C. Bradt, D. P. H. Hasselman, and F. F. Lange, eds., Plenum Press, New York, N.Y., pp. 613-646.
[31] Hartstock, D. L., 2002, "Ford's Development of the 820 High Temperature Ceramic Gas Turbine Engine," Ceramic Gas Turbine Design and Test Experience, M. van Roode, M. K. Ferber, and D. W. Richerson, eds., American Society of Mechanical Engineers, New York, N.Y., pp. 17-75.
[32] Yoshida, H., Chaudhri, M. M., Fukudome, T., and Tsuruzono, S., 2005, "Impact Fracture Behavior of Turbine-Grade Silicon Nitride Ceramic Under Tensile Stress at Elevated Temperatures," ASME Conference Proceedings, 2005(46997), pp. 241-245.
[33] Wilson, D. G., 1997, "A New Approach To Low-Cost High-Efficiency Automotive Gas Turbines," No. 970234, Society of Automotive Engineers, Warrendale, PA.
[34] Foster, S., 2007, "Personal communication," Kyocera Industrial Ceramic Components, Inc., Vancouver, WA.
[35] van Roode, M., Ferber, M. K., and Richerson, D. W., 2003, "Ceramic gas turbine component development and characterization," American Society of Mechanical Engineers, New York, NY.
[36] Wilson, D. G., 2002, "The basis for the prediction of high thermal efficiency in W.T.P.I. gas-turbine engines," Wilson Turbo Power Incorporated, Winchester, MA.
[37] McDonald, and C., 2003, "Recuperator considerations for future higher efficiency microturbines," Applied Thermal Engineering, 23(12), pp. 1463-1487.
[38] McDonald, C., and Rodgers, C., 2008, "Small recuperated ceramic microturbine demonstrator concept," Applied Thermal Engineering, 28(1), pp. 60-74.
[39] McDonald, C. F., 2003, "Recuperator considerations for future higher efficiency microturbines," Applied Thermal Engineering, 23(12), pp. 1463-1487.
[40] McDonald, C. F., 1990, "Gas turbine recuperator renaissance," Heat Recovery Systems and CHP, 10(1), pp. 1-30.
[41] McDonald, C. F., and Rodgers, C., 2002, "The Ubiquitous Personal Turbine—A Power Vision for the 21st Century," Journal of Engineering for Gas Turbines and Power, 124(4), p. 835.
[42] McDonald, C. F., and Wilson, D. G., 1996, "The utilization of recuperated and regenerated engine cycles for high-efficiency gas turbines in the 21st century," Applied Thermal Engineering, 16(8-9), pp. 635-653.
[43] Opila, E. J., and Hann, R. E., 1997, "Paralinear Oxidation of CVD SiC in Water Vapor," Journal of the American Ceramic Society, 80(1), pp. 197-205.

[44] Incropera, F. P., and DeWitt, D. P., 2002, Fundamentals of Heat and Mass Transfer, 5th Ed.

APPENDIX

The modified model (3) is readily deduced by returning to [2], which references Opila et al. [43], where the form of standard model (3) was originally derived. The authors started from an accepted correlation for gas diffusion through the boundary layer in laminar flow over a flat plate (e.g. [44], eqs. 7.32 and 7.27):

$$\frac{J_{avg}L}{D\rho_i} = .664\left(\frac{\rho VL}{\mu}\right)^{1/2}\left(\frac{\mu}{\rho D}\right)^{1/3} \quad (17)$$

$$\frac{J_{local}x}{D\rho_i} = .332\left(\frac{\rho Vx}{\mu}\right)^{1/2}\left(\frac{\mu}{\rho D}\right)^{1/3} \quad (18)$$

or equivalently, in dimensionless groups,

$$\overline{Sh_L} = .664\, Re_L^{1/2} Sc^{1/3} \quad (19)$$

$$Sh_x = .332 Re_x^{1/2} Sc^{1/3} \quad (20)$$

where

ρ is the concentration of the bulk gas mixture (kg/m^3)
ρ_i is concentration of the diffusing species at the surface
D is the mass diffusion coefficient (m^2/s)
μ is the gas viscosity (N·s/m^2)
J_{avg} is average mass flux of the diffusing species (kg/m^{2}s)
$\overline{Sh_L}$ is the dimensionless Sherwood number, $J_{avg}L/(D\rho_i)$
Sh_x is the local Sherwood number at position x
Re is the dimensionless Reynolds number $\rho VL/\mu$ or $\rho Vx/\mu$
Sc is the dimensionless Schmidt number, $\mu/(\rho D)$

In the Smialek reference, flux and species concentration terms J_{avg}, ρ, and ρ_i are denoted in molar units, e.g. ρ in mol/m^3, etc. However, they can equivalently be denoted in mass-basis units such as density (kg/m^3) by multiplying by the appropriate molecular weights, leading to more familiar forms of the dimensionless groups such as Reynolds number in (7).

In both Smialek et al.'s HPBR tests [2] and Opila et al.'s thermogravimetric experiments [43], surface recession was measured by weight. Therefore, these references began with the average mass transfer correlation (6) to derive the water vapor erosion model. Following [43], Smialek et al. then reason, essentially, that the diffusion coefficient $D \propto 1/P_{total}$; the gas density $\rho \propto P_{total}$; and the partial pressure of the diffusing species $P_{Si(OH)4} \propto P_{H2O}^2 \cdot exp(-Q/RT)$. Combining these observations with (6) above, they conclude that the recession rate is proportional to $exp(-Q/RT)\cdot V^{1/2}\cdot P_{H2O}^2 \cdot P_{total}^{-1/2}$, which is equivalent to (3).

However, algebraically, the streamwise sample length should also appear in this expression to the -½ power. For simplicity, this was omitted in references [2] and [43], and this worked, since all of the HPBR specimens and all of the TGA specimens had the same streamwise length. On the other hand, in the Rolls-Royce engine tests, the blade chord was different (2.7 cm), and the *local* recession rate at the trailing edge of the blade airfoils was measured, not the average over the entire surface. These differences are accounted for in (4) and (5), but not (3). The better agreement among B_2 values than B_1 values, and the better agreement with mass transfer theory, suggest the modified model should be used.

Equations (8) and (9) are exactly analogous to the familiar equation for convection heat transfer over a flat plate in laminar flow, e.g. $\overline{Nu_L} = .664 Re_L^{1/2} Pr^{1/3}$. In both cases, the boundary layer thickness grows in proportion to $\sqrt{x}$, where x is the distance downstream from the leading edge, and heat and mass fluxes are highest where the boundary layer is thinnest, at the leading edge. This explains why, for tests in which the local variation in erosion rates is observable, the erosion rate at the leading edge of each specimen is always greater than the average over the entire surface, while rates measured at the trailing edge are lower. A good example of this is shown in Figure 6 in [9].

Some limitations of the new model are as follows. First, it is suitable only for geometries that can be approximated as a flat plate in laminar flow, such as blade airfoils. For flow geometries that differ entirely from a flat plate, different correlations should be used. For example, to model recession in a heat exchanger, an internal flow correlation such as that for fully developed laminar flow in tubes might be suitable. Second, as with similar heat transfer correlations, the appearance of the streamwise position "x" in the denominator results in an infinite recession rate at the leading edge of the airfoil (x=0), which is incorrect. This is because airfoils are not infinitely thin flat plates. To model leading edge recession accurately, a different model that reflects the finite thickness and curvature would be needed. However, from mid-chord to the trailing edge, the new model proposed here should give reasonable approximations. Third, at higher Reynolds numbers, a turbulent flow correlation should be used. The Rolls-Royce 501-K first stage stator blades operate near the Reynolds number limit for laminar flow.

In summary, the only differences between the standard model (3) and the modified model (4),(5) are the appearance of the square root of the length term ($L^{0.5}$, $x^{0.5}$) in the denominator, and differentiation between the *average* recession rate over the entire surface and the *local* rate at a position x downstream from the leading edge. These changes improve the agreement among erosion rates measured in different series of tests. The adjustments also bring the standard model into better agreement with mass transfer theory. The revised model quantifies an observed variation in erosion rate with streamwise position on the specimen surface, with higher rates near the leading edge and lower rates near the trailing edge, which is not explained by the standard model. The new model is therefore recommended.